IEEE Access
Multidisciplinary | Rapid Review | Open Access Journal

Received December 7, 2020, accepted December 18, 2020, date of publication December 23, 2020, date of current version January 5, 2021.

Digital Object Identifier 10.1109/ACCESS.2020.3046754

Short-Term Photovoltaic Power Prediction Based on Similar Days and Improved SOA-DBN Model

WEI HU[1], XINYAN ZHANG[1], LIJUAN ZHU[2], AND ZHENEN LI[1]
[1]School of Electrical Engineering, Xinjiang University, Urumqi 830047, China
[2]School of Information Engineering, Xinjiang Institute of Technology, Aksu 843015, China

Corresponding author: Xinyan Zhang (xjcxzxy@126.com)

This work was supported by the National Natural Science Foundation of China under Grant 51667018.

ABSTRACT Existing methods in predicting short-term photovoltaic (PV) power have low accuracy and cannot satisfy actual demand. Thus, a prediction model based on similar days and seagull optimization algorithm (SOA) is proposed to optimize a deep belief network (DBN). Fast correlation-based filter (FCBF) method is used to select a meteorological feature set with the best correlation with PV output and avoid redundancy among meteorological factors affecting PV output. In addition, a comprehensive similarity index combining European distance and gray correlation degree is proposed to select the similar day. Then, SOA is used to optimize the number of neurons and the learning rate parameters in DBN. Based on the nonuniform mutation and opposition-based learning method, an improved seagull optimization algorithm (ISOA) with higher optimization accuracy is proposed. Finally, the ISOA-DBN prediction model is established, and the experimental analysis is conducted using the actual data of PV power stations in Australia. Results show that compared with DBN, support vector machine (SVM), extreme learning machine (ELM), radial basis function (RBF), Elman, and back propagation (BP), the mean absolute percentage error indicator of ISOA-DBN is only 1.512% on a sunny day, 5.975 on a rainy day, 3.359 on a cloudy to sunny day, and 1.911% on a sunny to cloudy day. Therefore, the good accuracy of the proposed model is verified.

INDEX TERMS PV power generation, prediction model, similar day, seagull optimization algorithm, deep belief network.

NOMENCLATURE

PV	photovoltaic
SOA	seagull optimization algorithm
DBN	deep belief network
FCBF	fast correlation-based filter
ISOA	improved seagull optimization algorithm
SVM	support vector machine
ELM	extreme learning machine
RBF	radial basis function
BP	back propagation
CEEMD	complementary ensemble empirical mode decomposition
SU	symmetric uncertainty
GR	global radiation
DR	diffused radiation
RBM	restricted Boltzmann machines
GBRBM	Gauss–Bernoulli-restricted Boltzmann machine
PSO	particle swarm optimization
GA	genetic algorithm
GOA	grasshopper optimization algorithm
RMSE	root mean square error
MAPE	mean absolute percent error

The associate editor coordinating the review of this manuscript and approving it for publication was Xiaodong Liang.

I. INTRODUCTION

The development and utilization of renewable energy has become an important measure for all countries to solve energy and environmental problems [1]. Clean PV energy has become a potential power resource in many parts of the world and has been developed vigorously [2], [3]. However, PV fluctuates greatly due to the impact of meteorological and environmental conditions, and its large-scale penetration brings many security challenges to the power grid system.

To improve the grid-connected access rate of PV power generation, various technologies, such as demand

response [4], [5], microgrid [6]–[8], unit optimization [9], distributed generation [10], energy storage [11]–[14], and PV power prediction, have emerged in the power system. Among them, short-term PV power generation power prediction can better evaluate the short-term operation state and development trend of PV power station. Therefore, accurate PV power prediction is greatly important for the effective resources utilization [15]–[16].

At present, understanding the short-term PV power prediction theory is still in the extensive research stage. Short-term PV power prediction methods include physical methods, statistical methods, and artificial intelligence algorithms. The physical method establishes a physical model to calculate the PV power generation output by referring to the basic principles of PV power generation and combining the detailed module parameters, geographic information, and numerical weather forecast data of PV power station [17]–[19]. The physical method is suitable for the prediction under stable conditions. When the meteorological condition changes rapidly, the prediction performance is greatly affected [20]. The statistical method relies on historical data, such as PV output and meteorology, to establish the mapping relationship. Statistical methods include time series method [21], gray theory [22], [23], and regression analysis method [24]. Such methods are relatively simple in modeling and suitable for linear series data with stable changes. However, the generalization ability of this method is poor for nonlinear data. Intelligence algorithms do not rely on predefined mathematical models. They obtain the prediction model through training the sample set. They are used in PV output prediction. Lin *et al.* [2] proposed a short-term PV prediction model based on Elman method and the optimal similarity date is determined by combining with the gray correlation analysis method. Wang *et al.* [25] proposed the Elman prediction model, and obtained the advantages of the proposed method through comparison with BP neural network. Lin *et al.* [26] proposed an improved moth-flame optimization algorithm, which was used to optimize support vector machine (SVM), and proved the good performance of the model in sunny and rainy days. Zhou *et al.* [27] proposed to optimize the ELM model with genetic algorithm and used the model to predict different seasons. Jiang *et al.* [28] proposed the combination model of fuzzy clustering and ELM, and verified the effectiveness of the model. Alsarraf *et al.* [29] proposed a method to optimize artificial neural network by particle swarm optimization (PSO), which realized the photovoltaic power prediction. Liu *et al.* [30] proposed to use the improved chicken swarm algorithm to improve the threshold of extreme learning machine (ELM), and verified the prediction function under different weather conditions. Niu *et al.* [31] proposed the complementary ensemble empirical mode decomposition (CEEMD) method, which reduces the fluctuation degree of the original sequence. Finally, the prediction is performed using the BP, and the effectiveness of the mixed model is verified. Yang *et al.* [32] proposed the use of a competitive swarm optimizer to optimize parameters of the RBF. They finally verified the effectiveness of the model. On the basis of the traditional cuckoo algorithm, Zhou *et al.* proposed [33] a two-mode cuckoo search algorithm, and an optimized wavelet neural network model is established. [34] used ant colony algorithm to optimize the SVM and realized accurate prediction in a very short term.

The traditional neural network prediction model is a shallow and has limited ability to express nonlinear complex functions. This type of model is prone to underfitting when dealing with complex prediction problems. Recently, a new artificial intelligence technology, namely, deep learning has emerged. The deep learning algorithm is an extension of the traditional artificial intelligence algorithm. By building a machine model with multiple hidden layers, it can learn and mine more useful features in the data. Thus, the prediction accuracy is improved. At present, deep learning technology has been used in load forecasting [35]–[37], wind power output forecasting [38]–[40], and other fields. It has achieved good prediction results. Zhang *et al.* [41] pointed out that the deep belief network (DBN) can effectively represent the internal structure of complex data and characteristics. Thus, the DBN model is used in the current research to forecast the short-term PV power. Fast correlation-based filter (FCBF) method is put forward, combining similar day and ISOA (improved seagull optimization algorithm)-DBN PV power prediction model. It is compared with radial basis function (RBF), BP, SVM, Elman, ELM, DBN, and other prediction models to show its superiority in prediction accuracy. The main contributions of this study include the following:

1) An FCBF method is proposed to screen significant meteorological factors corresponding to PV power generation.

2) A new method is proposed using the best similarity day (integrated gray correlation degree and Euclidean distance) and deep learning technology (DBN).

3) An improved seagull optimization algorithm is proposed and verified to optimize the structural parameters of DBN model.

4) The validity of the model is evaluated with the actual data in different weather types and seasons.

The remainder of this article is organized as follows. Section 2 analyzes the PV power generation and the meteorological feature set associated. Section 3 introduces standard depth belief networks and Gauss–Bernoulli constrained Boltzmann machines. Section 4 describes the implementation process of the ISOA-DBN prediction model. Section 5 carries on the experiment. The conclusions are drawn in Section 6.

II. SELECTION OF METEOROLOGICAL FEATURE VECTOR AND SIMILAR DAY

A. SELECTION OF METEOROLOGICAL FEATURE VECTORS

DKA PV power station data from Australia are used to obtain the generation power of the PV power station and corresponding meteorological data. Excessive noncritical factors increase the complexity of prediction and reduce the convergence speed. To reduce the nonrelated factors, extracting meteorological factors, which are more correlated with PV

power, is necessary to avoid the redundancy. The commonly used correlation feature extraction method is Pearson correlation coefficient method. However, this method can only measure the linear correlation degree between PV power generation and meteorological factors. It also ignores the redundancy among meteorological factors. FCBF is a typical feature selection method, which can not only measure the correlation between meteorological factors and PV power generation, but can also effectively avoid the redundancy among meteorological factors.

1) FORECAST MODEL INPUT METEOROLOGICAL FEATURE SET IS SCREENED USING THE FCBF ALGORITHM

FCBF uses symmetric uncertainty (SU) for feature selection, and the calculation formula is shown in reference [42]. The feature subset with the most significant category correlation is screened out and its redundant features are deleted by determining the correlation between features and categories and the relationship among these features. PV power generation is selected as the category, and global radiation, diffusion radiation, wind speed, wind direction, humidity, temperature, and other meteorological factors corresponding to PV power are selected as the characteristics. The characteristic quantity data set of PV power station is assumed $W = (w_{ij})_{N\times D}$, where x_{ij} is the ith data of the jth meteorological characteristic vector. N is 133, which represents the total number of sample points in the interval of a day from 7:00 to 18:00, and the interval between data time points is 5 minutes. D is 6 when no meteorological factor of rainfall exists; otherwise, the value is 7. The category vector of the PV power station is $P = (p_i)_{N\times 1}$, where p_i is the ith PV power category data of the corresponding weather vector x_{ij}. Then, the input feature selection method based on FCBF algorithm can be described as follows:

Step 1: Features that are weak or irrelevant are removed. The null sets G and Q are set, and the jth feature w_{Nj} in the meteorological feature data set W and the SU(w_{Nj};P) of the PV power category P are calculated. If SU(w_{Nj};P) $< \sigma$ (σ is the preset threshold of FCBF algorithm), then the feature w_{Nj} is deleted and the reserved meteorological features are placed into G.

Step 2: Redundancy features are screened. The special collection in G is arranged in descending order of SU(w_{Nj};P) size, and the maximum meteorological feature w_{Nj} is obtained and placed into Q. SU(w_{Nj};w_{Ni}) of the remaining candidate meteorological feature w_{Ni} in w_{Nj} and G is calculated. If SU(w_{Nj};w_{Ni}) $>$ SU(w_{Nj};P), then the meteorological features w_{Ni} are screened out of G.

Step 3: Step 2 is repeated and carried out step by step; finally, the filtered input meteorological feature set is obtained.

The preset threshold σ of the FCBF algorithm is set to 0.4. The meteorological characteristics of the prediction model screened by the FCBF algorithm are input global radiation (GR) and diffused radiation (DR), which constitute the meteorological feature vector C [X_{GR}, X_{DR}].

2) TIME-VARYING CURVES OF THE METEOROLOGICAL FACTORS AND PV POWER GENERATION

Two typical meteorological weathers, sunny day with less volatility and rainy day with greater volatility, are selected as examples, and their relationship is analyzed from the temporal variation curve. They are shown in Figures 1 and 2. The figures show that the GR, DR curve, and the PV power curve have evident correlation, which verifies the results obtained by the FCBF algorithm. The factors, such as rainfall, wind speed, wind direction, and humidity, have poor correlation with the PV power. The temperature has inertia characteristic, which cannot reflect the transient situation of power. Especially, the correlation between temperature and PV power is poor in the declining stage.

This analysis indicates that the model input meteorological feature set selected in the subsequent establishment of the prediction model includes GR and DR.

B. SELECTION OF SIMILAR DAYS

1) GRAY CORRELATION AND EUCLIDEAN DISTANCE

Gray correlation degree R_i can effectively analyze the situation changes between sequences; it can reflect the shape similarity between the meteorological feature vector C_i [X_{GR}, X_{DR}] on the ith historical day and the predicted day vector C_0 [X_{GR}, X_{DR}]. Then, the R_i calculation formula of global radiation GR and diffusion radiation DR is defined as follows:

$$R_i = \frac{1}{l}\sum_{k=1}^{l}\omega_1\varepsilon_i(k) + \frac{1}{l}\sum_{k=1}^{l}(1-\omega_1)\varepsilon_i(k) \tag{1}$$

where ω_1 and $(1-\omega_1)$ are the weights of GR and DR, respectively; l refers to the number of elements of a single meteorological feature vector in the time interval of a day from 7:00 to 18:00; it is the same as in the previous study, that is, 133. $\varepsilon_i(k)$ is the correlation coefficient between the kth elements corresponding to the predicted day and the ith historical day. Formula is as follows:

$$\varepsilon_i(k) = \frac{\min\limits_i\min\limits_k\left|x'(k)-x_i'(k)\right| + \rho\max\limits_i\min\limits_k\left|x'(k)-x_i'(k)\right|}{\left|x'(k)-x_i'(k)\right| + \rho\max\limits_i\max\limits_k\left|x'(k)-x_i'(k)\right|} \tag{2}$$

where $x'(k)$ and $x_i'(k)$ are the kth meteorological element of the normalized forecast day and the ith historical day, respectively; ρ is a constant, that is, 0.5.

The Euclidean distance D_i can measure the distance between sequences, and it can reflect the position relationship between the meteorological vector of a certain historical day and the predicted day vector. Then, the calculation formula of D_i integrating GR and DR is defined as follows:

$$D_i = \sqrt{\sum_{k=1}^{l}\omega_1[x_0(k)-x_i(k)]^2} + \sqrt{\sum_{k=1}^{l}(1-\omega_1)[x_0(k)-x_i(k)]^2} \tag{3}$$

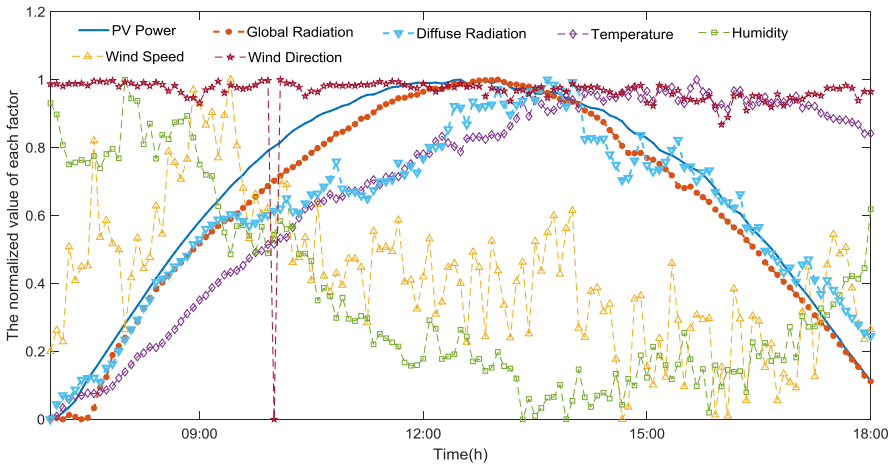

FIGURE 1. PV power and corresponding meteorological factors in sunny day.

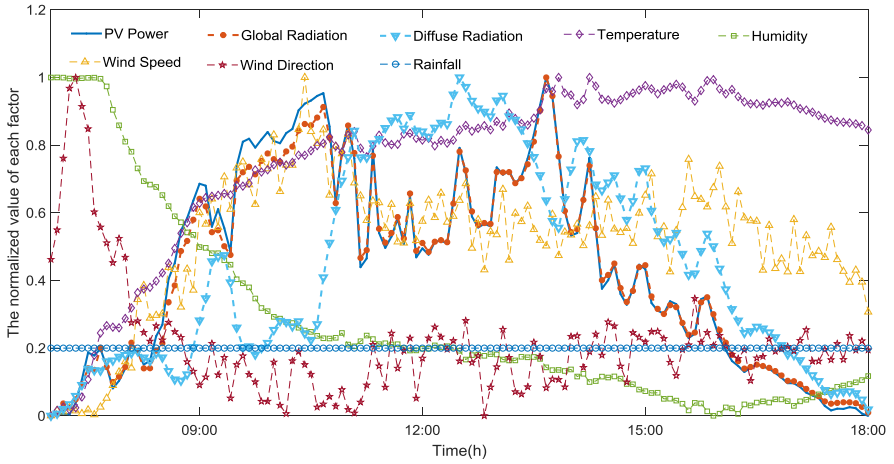

FIGURE 2. PV power and corresponding meteorological factors in rainy day.

where the values of l and ω_1 are the same as in the previous study.

2) WEIGHT CALCULATION

The combination of meteorological characteristics composed of GR and DR has different correlations with PV power generation and requires a reasonable distribution of the weight ω_1 in equations (1) and (3). The subjective weighting method [43] is limited by the knowledge and experience of experts and has a large subjective randomness defect. Therefore, the standard deviation method in the objective weighting approach is adopted to determine the weights of GR and DR. Each historical day has two meteorological features, such as GR and DR, and the element number of each meteorological feature is 133, forming a matrix $X = [x_{ij}]_{133\times 2}$. x_{ij} represents the ith element value of the jth meteorological feature in a historical day. The formula for calculating the weight of each factor by using the standard deviation method is as follows:

$$S_j = \sqrt{\frac{\sum_{i=k}^{l}(x_{ij} - \bar{x}_j)^2}{l-1}} \quad (\mathrm{j} = 1, 2) \tag{4}$$

where S is the sample standard deviation of meteorological feature; $\bar{x}$ is the sample mean value of meteorological feature.

The weight of the jth meteorological feature is as follows:

$$\omega_j = \frac{S_j}{\sum_{j=1}^{2} S_j} \quad (\mathrm{j} = 1, 2) \tag{5}$$

where $\omega \in [0, 1]$, and $\omega_1 + \omega_2 = 1$.

3) COMPREHENSIVE SIMILARITY

To accurately select the most similar historical date to the predicted date, the Euclidian distance combined with the gray relational analysis method is used to construct the comprehensive similarity index Z_i. Its calculation formula is as follows:

$$Z_i = \alpha \frac{\min\limits_{1\le i\le n}(D_i)}{D_i} + \beta \frac{R_i}{\max\limits_{1\le i\le n}(R_i)} \tag{6}$$

where α and β are empirical weight coefficients, both of which are set to 0.5. Historical PV power generation days

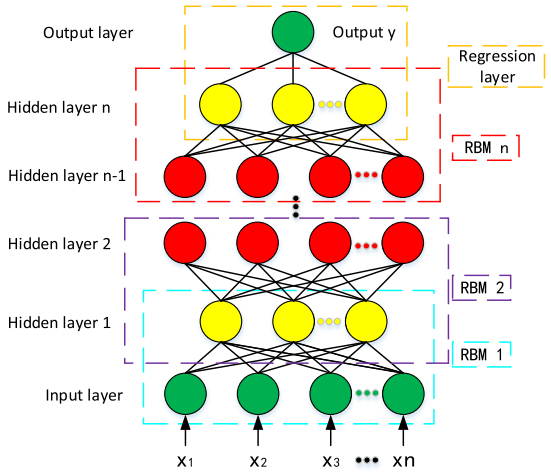

FIGURE 3. Structure of DBN.

with similarity $Z_i \geq 0.8$ are selected by date; b days close to the predicted date are selected as similar days, and b = 5.

III. DBN NEURAL NETWORK

A. STANDARD DBN

DBN is proposed by Goeffrey Hinton [44], [45], and its structure is shown in Figure 3. It is composed of multiple stacked restricted Boltzmann machines (RBM). The RBM model is fully connected between layers, and no connection exists within the layers. The output layer of the previous RBM is the input layer of the next RBM unit. A regression layer is constructed by a hidden layer and an output layer at the end of the entire network structure. Through vector x and vector y, the set {x,y} of the prediction model is constituted.

The combined configuration energy function of the visible layer and the hidden layer is as follows:

$$E(v, h\,|\theta\,) = -\sum_{ij} w_{ij} v_i h_j - \sum_i a_i v_i - \sum_j b_j h_j \qquad (7)$$

where v_i and h_j represent the states of visible layer nodes and hidden layer nodes, respectively; a_i and b_j represent the bias; w_{ij} represents the connection weight between the visible and hidden layers.

In accordance with the above formula, the joint probability density can be obtained as follows:

$$p(v, h\,|\theta\,) = \frac{1}{Z(\theta)} e^{-E(v,h|\theta\,)} \qquad (8)$$

where $Z(\theta)$ is the normalized factor.

For the training set containing N samples, the maximum likelihood function can be used to obtain the following:

$$\theta^* = \arg\max_{\theta} L(\theta) = \arg\max_{\theta} \sum_{n=1}^{N} \log p(v^n\,|\theta\,) \qquad (9)$$

DBN algorithm pretrains RBM layer by layer, and then uses the supervised BP algorithm to fine-adjust and optimize the initial weight obtained from pretraining layer by layer, so that the model can obtain the optimal solution, and thus can represent the complex nonlinear relationship in the PV data.

B. GAUSS-BERNOULLI LIMITED BOLTZMANN MACHINE

Because the hidden layer and the visible layer nodes of the standard DBN are Bernoulli values at the time of sampling, the input variables are continuous data at the time of PV power prediction. Therefore, Gauss–Bernoulli-restricted Boltzmann machine (GBRBM) is introduced as the first RBM of DBN PV prediction model. The continuous input data are converted into binary Bernoulli variables by GBRBM, and then further processed by standard RBM. This DBN can process continuous data and has the ability to model functions. The energy function of GBRBM is as follows:

$$E(v, h\,|\theta\,) = -\sum_{ij} \frac{v_i}{\sigma_i} w_{ij} h_j - \sum_i \frac{(v_i - a_i)^2}{2\sigma_i^2} - \sum_j b_j h_j \qquad (10)$$

In the formula, v_i and h_j represent the states of the visible layer node and the hidden layer node, respectively. At this point, v_i belongs to the actual value input vector of PV power correlation factor, h_j value still conforms to Bernoulli type {0, 1} distribution, and σ is the standard deviation of Gaussian distribution. According to Equations (11) and (12), the conditional probability can be obtained.

$$p(v_i\,|h\,) = N(a_i + \sigma_i \sum_j w_{ij} h_j, \sigma_i^2) \qquad (11)$$

$$p(h_j = 1\,|v\,) = \text{sigmoid}(b_j + \sum_i \frac{v_i}{\sigma_i} w_{ij}) \qquad (12)$$

where $N(\mu, \sigma_i)$ is a Gaussian function with a mean value of μ and a standard deviation of σ.

IV. PV POWER GENERATION POWER PREDICTION MODEL BASED ON ISOA-DBN

Literature [46] points out that setting appropriate parameters has an important impact on the modeling accuracy of DBN for specific sample data and the DBN structure. Moreover, factors, such as the number of hidden layers, the number of neurons in each layer, and the learning rate in DBN, are analyzed. Therefore, the number of hidden layers in the deep neural network should be set to two or three, and the model accuracy is relatively high. When the number of hidden layers increases to four, the classification or prediction effect of the model and the generalization performance decrease. To save the algorithm time, the DBN network structure with two hidden layers is selected, and the improved seagull optimization algorithm is used to optimize the number of neurons in the two hidden layers and the learning rate of the entire DBN network.

A. SOA

SOA is a new intelligent algorithm proposed by Gaurav Dhiman. It simulates the migration and attack behavior of seagulls and shows better performance in solving optimization constraint problems compared with common PSO,

genetic algorithm(GA), locust algorithm, and other optimization algorithms [47].

1) MIGRATION

Migration indicates that the algorithm simulates the movement of the seagull population from one place to another.

① Avoid collisions. The additional variable A is adopted to calculate the new position of seagulls.

$$C_s = A \times p_s(x) \tag{13}$$

where C_s represents the new position that does not conflict with other seagulls, $p_s(x)$ represents the current position of seagulls, and A represents the movement behavior of seagulls.

$$A = f_c - (t \times (f_c / Max_{\text{interation}})) \tag{14}$$

where f_c is used to control the range of the variable A, and $Max_{\text{interation}}$ represents the maximum number of iterations.

② Optimal position direction. After avoiding collisions between neighboring gulls, the gulls move toward the optimal position.

$$M_s = B \times (P_{bs}(x) - P_s(x)) \tag{15}$$

where M_s is the direction of the optimal position; $P_{bs}(x)$ is the best seagull position; B is a random number within the range of [0,1], which is mainly used to balance global and local search.

$$B = 2 \times A^2 \times r_d \tag{16}$$

③ Close to the best position. The seagull moves in the direction of the best position to reach the new position D_s.

$$D_s = |C_s - M_s| \tag{17}$$

2) ATTACK

When a seagull finds its prey, it attacks the target in a spiral motion by constantly changing its attack angle and speed. Planes x, y, and z can be described as follows:

$$x = r \times \cos\theta \tag{18}$$

$$y = r \times \sin\theta \tag{19}$$

$$z = r \times \theta \tag{20}$$

$$r = u \times e^{\theta v} \tag{21}$$

where r is the radius of one circle of the helix; θ is a random value within the range of $[0, 2\pi]$; u and v are constants that define the shape of the helix. The attack position P_s of the seagull can be obtained from the following equation:

$$P_s = D_s \times x \times y \times z + P_{bs} \tag{22}$$

B. IMPROVED SEAGULL OPTIMIZER ALGORITHM

SOA has the advantages of easy implementation, but the algorithm is still prone to premature convergence and other disadvantages. This study proposes an improved SOA (ISOA) to solve the existing problems of the traditional SOA.

The seagull algorithm randomly determines the initial position of the seagull. If the initial value generated randomly is unfavorable, then it affects the final experimental results. Therefore, Chaotic mapping is proposed to generate the initial population of seagull. Chaos is a random and irregular motion that occurs in a deterministic system. A chaotic variable has the characteristics of randomness, ergodicity, and regularity in a certain range. Thus, the chaotic property is helpful to enhance the search diversity. The widely used logistic map is selected as the chaos model to improve the initial value of the population. The model is shown as follows:

$$x_{n+1} = \mu \times x_n \times (1 - x_n), \quad t = 0, 1, 2 \cdots \tag{23}$$

where μ is the control variable, which determines the degree of chaos in the logistic mapping. The greater μ value indicates higher degree of chaos, which is generally valued between [0,4] and $x_n \in [0, 1]$.

The nonuniform mutation method is a type of automatic adjustment of search step size, which can effectively avoid SOA falling into local optimal and premature. The principle is as follows: suppose that variation operation is performed on the kth component of vector $X_i = (x_{i1}, x_{i2}, \cdots, x_{ik}, \cdots, x_{im})$, and the upper and lower bounds of x_{ik} are denoted as UB and LB, respectively. Then, the component after variation is as follows:

$$x'_{id} = \begin{cases} x_{id} + \Delta(t, UB - x_{id}), & \text{r} < 0.5 \\ x_{id} - \Delta(t, x_{id} - LB), & \text{r} \geq 0.5 \end{cases} \tag{24}$$

where t is an iteration variable; T is the maximum number of iterations; r is a random value in the [0, 1] range; b is the system parameter. Nonuniform variation step size $\Delta(t, y)$ is a mutation operator that can be adaptively adjusted. It enables the program to scan the entire search space in a wide range in the first half, thereby ensuring the global exploration ability and avoiding premature local optimal solutions. With the increase in iteration variables, the step size of the nonuniform variation gradually decreases to realize the convergence to the optimal solution.

The basic idea of opposition-based learning is to find the reverse solution of a feasible solution, evaluate the original solution and the reverse solution at the same time, and select and save a better solution. [48] pointed out that the reverse solution has greater probability of approaching the global optimal solution than the random solution. Thus, it can be used to improve the efficiency of SOA optimization. Variation operation is performed on the j component of vector $X_i = (x_{i1}, x_{i2}, \cdots, x_{ij}, \cdots, x_{im})$, and the upper and lower bounds of x_{ij} are denoted as $x_{\max j}$ and $x_{\min j}$, respectively. Then, the component after reverse learning is as follows:

$$x^*_{ij} = x_{\min j} + x_{\max j} - x_{ij} \tag{25}$$

The process of improving the seagull optimizer is as follows:

Step 1. Parameter initialization. The population size is set as N, the spatial dimension of the seagull search is set as v,

TABLE 1. Test functions.

Functions	Dimension	Value range	Optimal
$f_1(x)=\sum_{i=1}^{n}x_i^2$	30	[-100,100]	0
$f_2(x)=\sum_{i=1}^{n}\lvert x_i\rvert+\prod_{i=1}^{n}\lvert x_i\rvert$	30	[-10,10]	0
$f_3(x)=\sum_{i=1}^{n}(\sum_{j-1}^{i}x_j)^2$	30	[-100,100]	0
$f_4(x)=\sum_{i=1}^{n}[x_i^2-10\cos(2\pi x_i)+10]$	30	[-5.12,5.12]	0
$f_5(x)=-20\exp(-0.2\sqrt{\frac{1}{n}\sum_{i=1}^{n}x_i^2})-\exp(\frac{1}{n}\sum_{i=1}^{n}\cos(2\pi x_i))+20+e$	30	[-32,32]	0
$f_6(x)=\frac{1}{4000}\sum_{i=1}^{n}x_i^2-\prod_{i=1}^{n}\cos(\frac{x_i}{\sqrt{i}})+1$	30	[-600,600]	0

the chaos control parameter is set as μ, and the number of iterations is set as T.

Step 2. Producing the chaotic sequence z_{1D}. A set of variables $z_{1D} = [z_{11}, z_{12}, \cdots, z_{1D}]$ whose value interval is [0,1] are randomly generated, and $N-1$ chaotic variables $z_{2D}, z_{3D}, \cdots, z_{ND}$ are generated by Logistic mapping.

Step 3. Generation of the population. According to the following formula, N variables are mapped to $[x_{\min j}, x_{\max j}]$, which is the value interval of the seagull search.

$$x_{ij} = x_{\min j}+Z_{kj}(x_{\max j}-x_{\min j}), \quad i=1, 2, \cdots; \ j=1, 2, \cdots \tag{26}$$

Step 4. Twin group parallel search. The entire population N was divided into two subgroups of $N/2$. Seagull uses formulas (13)–(22) to form its own optimization subgroup and formula (24) to form the nonuniform variation subgroup to improve the global search capability of SOA.

Step 5. The reverse learning formula (25) is used to obtain the newly generated reverse learning population of the two subgroups.

Step 6. The fitness function is used to evaluate the optimal seagull population, the nonuniform variation population, and the two reverse populations in Step 5, and the individual with highest fitness is selected as the optimal individual.

Step 7. Steps 4–6 are repeated, and the algorithm is ended when it reaches or satisfies the accuracy requirements to obtain the optimal solution.

The ISOA algorithm flow is shown in Figure 4.

To verify the performance of the proposed ISOA, six classical test functions with different optimization characteristics were selected for the comparative analysis of the original SOA, PSO, and grasshopper optimization algorithm (GOA). The test function is shown in Table 1, where $f_1 \sim f_3$ is a unimodal function used for testing the convergence accuracy of the algorithm, and X2 is a multipeak function used for inspect the algorithm's ability to avoid the local optimal. The Settings of each algorithm are shown in Table 2. The calculation results are evaluated by four performance indicators. The results of the algorithm running independently for 30 times are shown in Table 3. The test results show that the

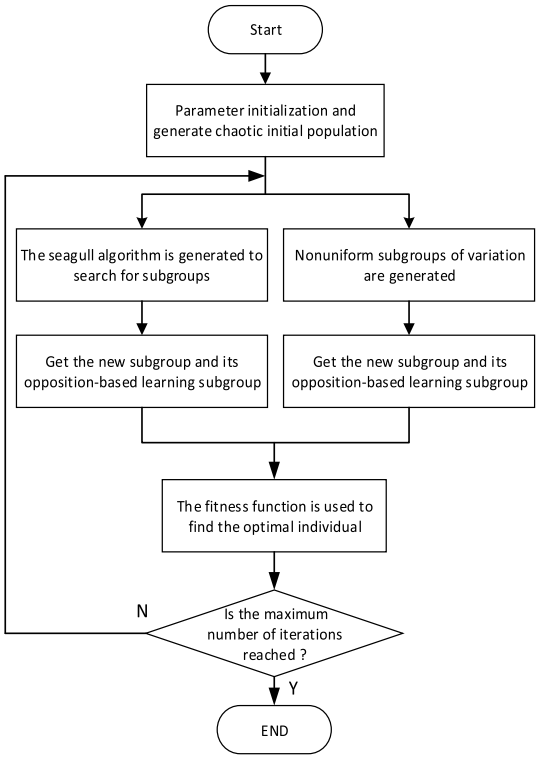

FIGURE 4. SOA algorithm flow chart.

convergence accuracy of the ISOA algorithm is better than that of the SOA, PSO, and GOA algorithms for the unimodal test function. The PSO algorithm has poor test results on f_3 function, but the test accuracy of f_2 is better than that of GOA algorithm. The test results of the SOA algorithm are better than those of PSO and GOA. For the multipeak test functions, the ISOA algorithm obtains the theoretical optimal value 0 for functions f_4 and f_6, and its convergence accuracy in the multipeak function tests is better than that of SOA, PSO, and GOA algorithms. The optimization results of the SOA, PSO, and GOA algorithms in the multipeak function test are unstable. In summary, the ISOA algorithm has higher accuracy than the three other algorithms, thereby showing better optimization ability and stability.

TABLE 2. Parameter settings.

Algorithms	Parameter
PSO	N=100，M=500，c1=c2=1.4962，w=0.7298
GOA	N=100，M=500
SOA	N=100，M=500
ISOA	N=100，M=500

TABLE 3. Test results.

Functions	Algorithms	Optimal	Worst	Average	standard deviation
f_1	PSO	6.0021e-06	1.766e-05	1.1107e-05	4.8681e-06
	GOA	4.6808e-09	4.0897e-08	2.2136e-08	1.4813e-08
	SOA	2.7723e-16	1.4783e-14	7.8461e-15	5.9388e-15
	ISOA	4.9179e-24	7.1481e-21	2.4133e-21	3.3481e-21
f_2	PSO	0.0026	0.0059	0.0044	0.0013
	GOA	0.0473	1.0289	0.6430	0.4273
	SOA	1.9593e-10	5.4891e-10	3.7125e-10	1.4411e-10
	ISOA	6.4413e-14	7.4899e-13	3.1746e-13	3.0664e-13
f_3	PSO	26.2882	44.9213	35.5102	7.6081
	GOA	8.1717e-08	1.4393e-06	7.8831e-07	5.5562e-07
	SOA	6.0663e-09	5.2834e-08	3.2097e-08	1.9456e-08
	ISOA	6.1691e-11	6.8748e-09	2.5834e-09	3.0499e-09
f_4	PSO	26.8716	36.2813	30.7176	4.0289
	GOA	1.5426	3.2718	2.4228	0.7062
	SOA	6.2528e-13	2.4443e-12	1.6379e-12	7.5680e-13
	ISOA	0	0	0	0
f_5	PSO	0.0010	0.0041	0.0026	0.0012
	GOA	3.6296e-05	0.0001	3.1209e-04	3.4597e-04
	SOA	19.9555	19.9612	19.9459	0.0177
	ISOA	4.13e-13	3.312e-12	1.7790e-12	1.1893e-12
f_6	PSO	6.2831e-07	1.9531e-06	1.2448e-06	5.4471e-07
	GOA	0.0523	0.1724	0.1057	0.0499
	SOA	6.7724e-15	4.2855e-14	2.0160e-14	1.6133e-14
	ISOA	0	0	0	0

C. PREDICTION MODEL OF ISOA-DBN

For the two hidden layers of, the number of neurons in each hidden layer is expressed as m_1 and m_2, and the learning rate is η. When the seagull population in the ISOA algorithm is coded, each individual is a vector $\mathrm{X}(m_1, m_2, \eta)$, and the optimization problem of DBN parameter can be expressed as follows:

$$F_{fitness}(m_1, m_2, \eta) = \frac{\sum_{i=1}^{N} (y_i - Y_i)^2}{N}$$
$$\text{s.t.} \begin{cases} 1 \le m_1 \le 100 \\ 1 \le m_2 \le 100 \\ 0 \le \eta \le 1 \end{cases} \tag{27}$$

where N is the number of samples, and y_i and Y_i are the predicted and true values of the ith sample, respectively.

The process of using the ISOA to optimize the DBN model is shown in Figure 5.

Step 1. The DKA PV power station data, query singular values, and missing data in the data are preprocessed, and cubic spline interpolation is used for filling.

Step 2. The FCBF method mentioned is used to extract meteorological factors that are highly correlated with PV power and to remove redundant meteorological factors.

Step 3. The comprehensive similarity index is adopted to select the historical date that is most similar to the predicted date.

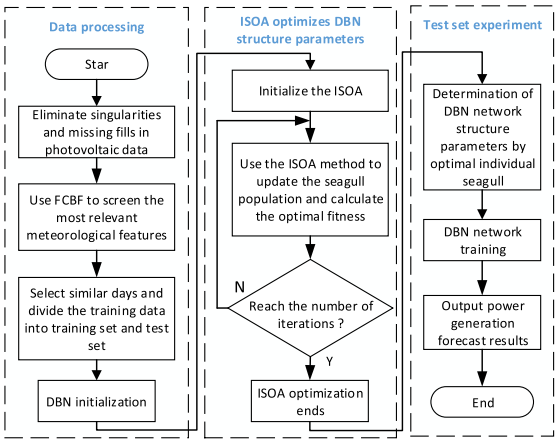

FIGURE 5. PV power prediction process based on ISOA-DBN model.

Step 4. The parameters, such as hidden layer number, training times, ISOA population number, and training times of the DBN network are initialized. The ISOA algorithm is used to determine the number of neurons and learning rate.

Step 5. The determined DBN network structure is pre-trained and reversely fine-tuned, and the DBN network training and test data are used to output the PV power forecast value.

TABLE 4. Forecast model input/output variables.

Input/output variables	Variable name
X1-x5	Power generation at the predicted time in a similar day
X6-x10	GR of the corresponding forecast time in a similar day
X11-x15	DR of the corresponding forecast time in a similar day
X16	GR at predicted moment
X17	DR at predicted moment
Y	Power generation at predicted moment

TABLE 5. Predictive model parameter settings.

Model	Parameter configuration
ISOA-DBN	The structural parameters: 19-64-36-1; learning rate:0.77; the maximum number of iterations:500
DBN	The structural parameters: 19-90-50-1; learning rate:1; the maximum number of iterations:500
SVM	RBF kernel function; solving penalty and kernel function parameters with grid search method, parameter range:[-8,8]
ELM	The structural parameters: 19-30-1; the maximum number of iterations:1000; activation function type: sig
RBF	The structural parameters: 19-30-1; the maximum number of iterations:1000
BP	The structural parameters: 19-20-1; learning rate:0.05; the maximum number of iterations:1000
Elman	The structural parameters: 19-30-1; the maximum number of iterations:1000

V. EXAMPLE ANALYSIS

A. BUILDING THE SAMPLE SET

The data of Alice Springs station in the DKA solar power center in Australia are used for the experiments. The selected sample data include the PV power data and corresponding meteorological data in the time interval from March 1, 2015 to March 1, 2016, and the resolution of the data is five minutes. The PV power at night is 0; thus, the PV power in the time period from 07:00 to 18:00 on the forecast day is selected for prediction. There are 133 sampling points in the whole day. According to the determination method of similar days in the above chapter, 5 historical days similar to the predicted days are selected as training samples, and 133 power values of the predicted days are tested. In accordance with the analysis results of PV power influencing factors, the input variables of the forecast model are determined as the PV power generation on similar days, global radiation GR, and diffuse radiation DR. The input and output variables of the prediction model are shown in Table 4.

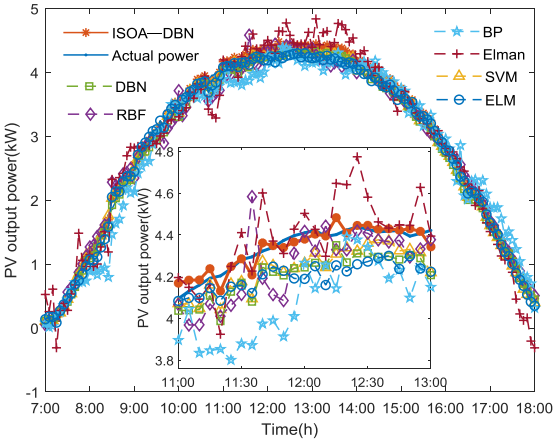

FIGURE 6. Forecast result of sunny day.

B. PARAMETER SETTING OF PREDICTION MODEL

The MATLAB R2019b is used as the test platform in a 64-bit Intel I5-3230M computer configuration. In the ISOA algorithm, the dimension is set to 3, the number of population is 30, and the maximum number of iterations is 100.After optimization by ISOA hidden layer neurons, the parameter optimization results of DBN are shown in Table 5.

To verify the effectiveness of the proposed algorithm, seven PV prediction models including BP, SVM, DBN, Elman, ELM, ISOA-DBN, and RBF are selected for comparative analysis. The proposed method is used for the similar day selection of each model, and the corresponding input and output variables are the same. In order to ensure objectivity, the parameters of each comparison model are set through trial and error method, and the comparative analysis is done for many times. Finally, the optimal parameter value is adopted. The parameter settings of each prediction model are shown in Table 5. The remaining parameters take the default values of the model.

C. ANALYSIS OF RESULTS

Four representative weather types, namely, sunny, rainy, sunny to cloudy, and cloudy to sunny are selected as the research objects. The dates are March 26 (sunny), June 17 (rainy), June 25 (cloudy to sunny), and August 25 (sunny to cloudy). The results of the following prediction models after 20 times of execution are averaged to avoid possible large fluctuation. The forecast and actual values of PV power generation under different weather types are shown in Figures 6–13.

Figures 6 and 7 show the result of sunny weather forecast. The figures show that the prediction results of the proposed model, ISOA-DBN, are better than those of the six other models. The prediction results of DBN, SVM, ELM, and RBF models are also ideal. The prediction results of the BP and Elman models are compared with other prediction models. The error graph shows that the prediction effect of these

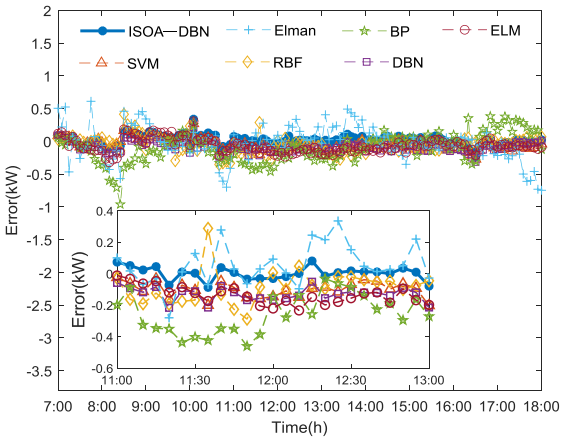

FIGURE 7. Forecast error of sunny day.

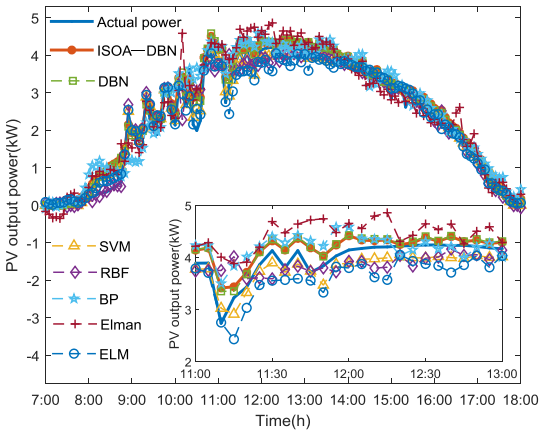

FIGURE 10. Forecast result of cloudy to sunny weather.

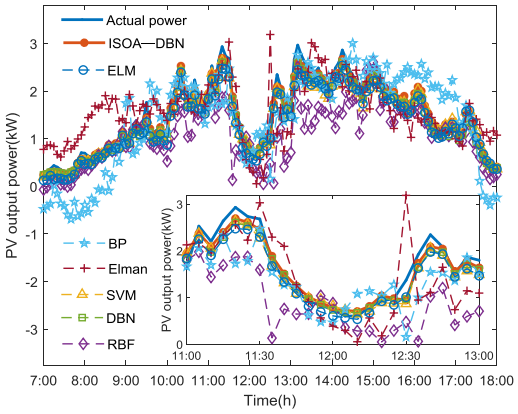

FIGURE 8. Prediction result of rainy day.

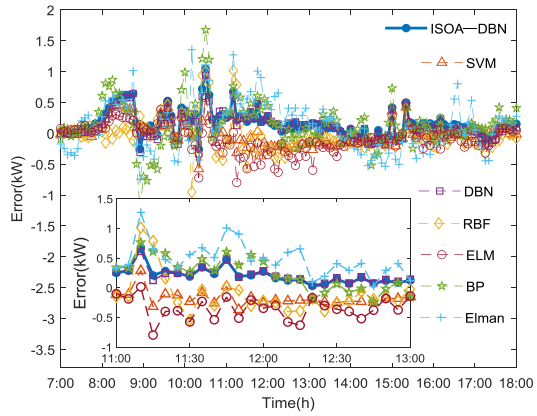

FIGURE 11. Forecast error of cloudy to sunny weather.

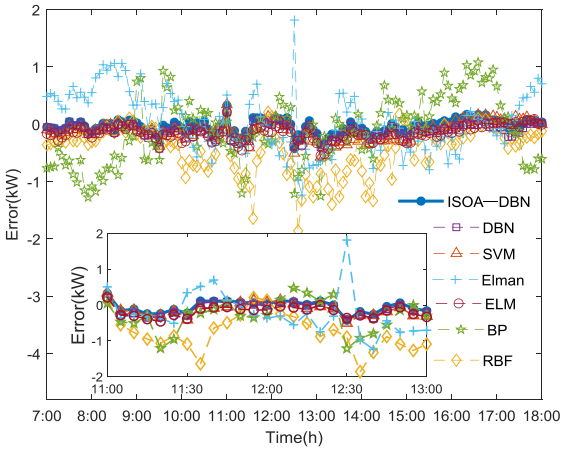

FIGURE 9. Prediction error of rainy day.

models has slight deviation from the actual value because the PV power generation power is regular and has less volatility on sunny days.

Figures 8 and 9 show the rainy weather forecast results. The figures show that the prediction effects of the seven models are worse than those in sunny days because the power fluctuates greatly in rainy days, thereby increasing the difficulty of prediction. However, compared with the six other models, ISOA-DBN shows better robustness, and the prediction effect is closer to the actual value. DBN, SVM, and ELM obtain better prediction results.

Figures 10 and 11 show the forecast results from cloudy to clear weather. The figures show that the prediction deviations of each model during the cloudy period from 08:00 to 12:00 are larger than the prediction deviations from 12:00 to 18:00 during the sunny period. This finding is due to the movement of clouds that causes the PV power station to generate electricity. The power fluctuation becomes larger, thereby increasing the difficulty of prediction. The prediction effect of the proposed ISOA-DBN is better than that of the six other models, DBN, SVM, and RBF have relatively better prediction effect.

Figures 12 and 13 show the forecast results under sunny to cloudy weather. The figures show that the prediction result is similar to that of cloudy to sunny weather. Similarly, the prediction effect is better during the sunny period from 07:00 to 14:00. However, during the cloudy period from 14:00 to 18:00, the actual PV power fluctuation law becomes worse due to the cloud movement, thereby reducing the prediction accuracy. The prediction effect of the proposed ISOA-DBN in sunny and cloudy periods is also better than that of the six

TABLE 6. Prediction error indexes under different weather.

Weather types	Error	ISOA-DBN	DBN	SVM	ELM	RBF	Elman	BP
Sunny	RMSE(MW)	0.075	0.086	0.098	0.112	0.125	0.243	0.352
	MAPE(%)	1.512	2.034	2.321	2.321	3.088	4.79	5.103
Rain	RMSE(MW)	0.124	0.159	0.196	0.204	0.596	0.517	0.586
	MAPE(%)	5.975	8.223	10.268	10.715	29.946	20.899	22.527
Cloudy to sunny	RMSE(MW)	0.196	0.210	0.237	0.25	0.268	0.411	0.4
	MAPE(%)	3.359	5.098	4.7	6.765	6.237	9.861	7.561
Sunny to cloudy	RMSE(MW)	0.103	0.123	0.147	0.133	0.548	0.322	0.283
	MAPE(%)	1.911	2.599	2.6607	2.985	9.285	7.53	6.905

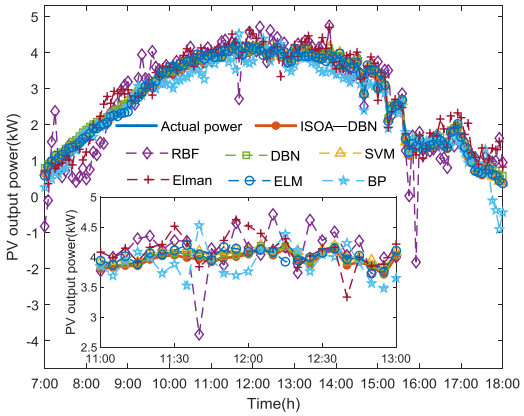

FIGURE 12. Forecast result of sunny to cloudy weather.

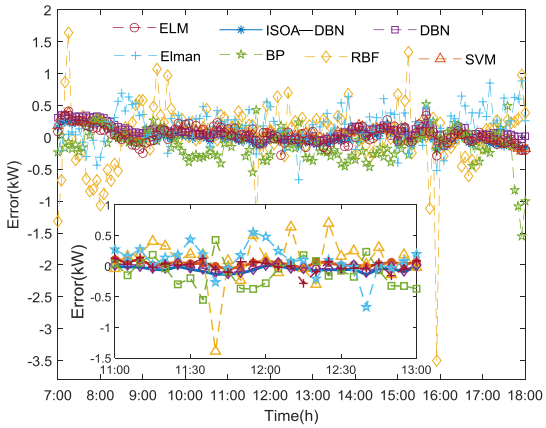

FIGURE 13. Forecast error of sunny to cloudy weather.

other models, among which DBN, SVM, and ELM models have relatively better prediction effect.

To accurately evaluate the prediction performance of various algorithms, two indexes, namely, root mean square error (RMSE) and mean absolute percent error (MAPE) are used to quantitatively analyze the prediction effect of each model.

$$\mathrm{RMSE} = \sqrt{\frac{1}{N}\sum_{i=1}^{N}\left(s_i - s_i'\right)^2} \tag{28}$$

$$\mathrm{MAPE} = \frac{1}{N}\sum_{i=1}^{N}\left|\frac{s_i - s_i'}{s_i}\right| \times 100\% \tag{29}$$

where N is the number of samples; s_i is the ith sample true value; s_i' is the ith sample prediction.

The quantified results of the prediction errors corresponding to the four types of weather are shown in Table 6. It shows that in sunny days with stable power change, the prediction effect of the seven forecasting methods is better than that of rainy days, cloudy to sunny days and sunny to cloudy days. The RMSE and MAPE of all model prediction errors are small, and the prediction results are relatively accurate. In rainy days, the randomness and volatility of power generation are large, and the RMSE and MAPE errors of all models are greater than those of the three other weather types. The RMSE and MAPE of the prediction errors in cloudy to sunny and cloudy periods are greater than those in sunny days because the appearance and movement of clouds in cloudy periods reduce the prediction accuracy of each method. Among the four weather types, the proposed ISOA-DBN method has smaller error quantization value, and its prediction effect is better than the six other methods; it has good environmental adaptability. At the same time, it can be known from the experimental error index value. When input variables and structural parameters of prediction model are determined, RMSE and MAPE values of ISOA-DBN, DBN and SVM methods are all fixed values. They have good predictive stability. However, when the other methods are used under the same conditions for multiple predictions, the results of each prediction vary in amplitude and have poor stability.

To verify the generalization ability of various algorithms in different seasons, the sunny weather is considered an example. In accordance with the classification standard of Australian seasons, one sunny day is selected from the four seasons of autumn, winter, spring, and summer as the forecast day. The forecast dates are April 24 (autumn), July 8 (winter), October 23 (spring), and December 5 (winter), and the forecast results and error indicators are shown in Figures 14-15 and Table 7, respectively. The prediction results of the

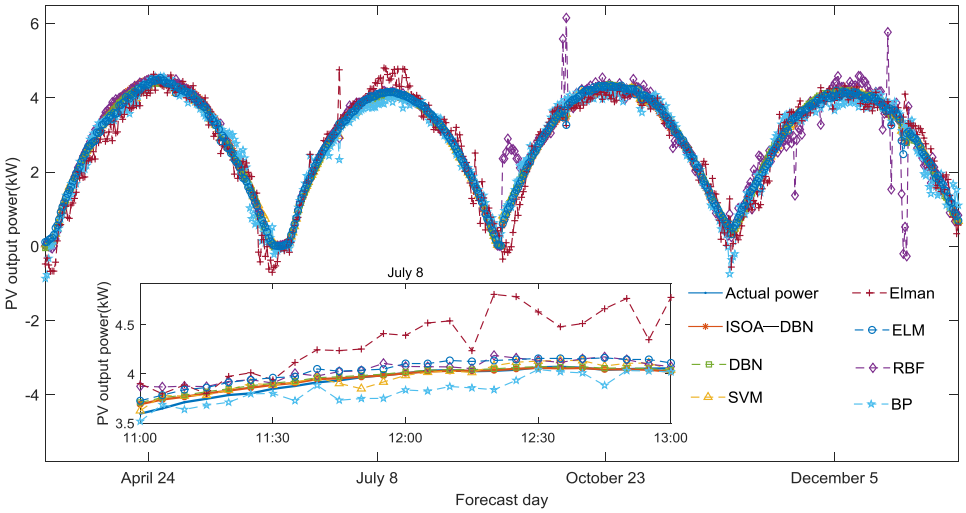

FIGURE 14. Prediction result of different seasons.

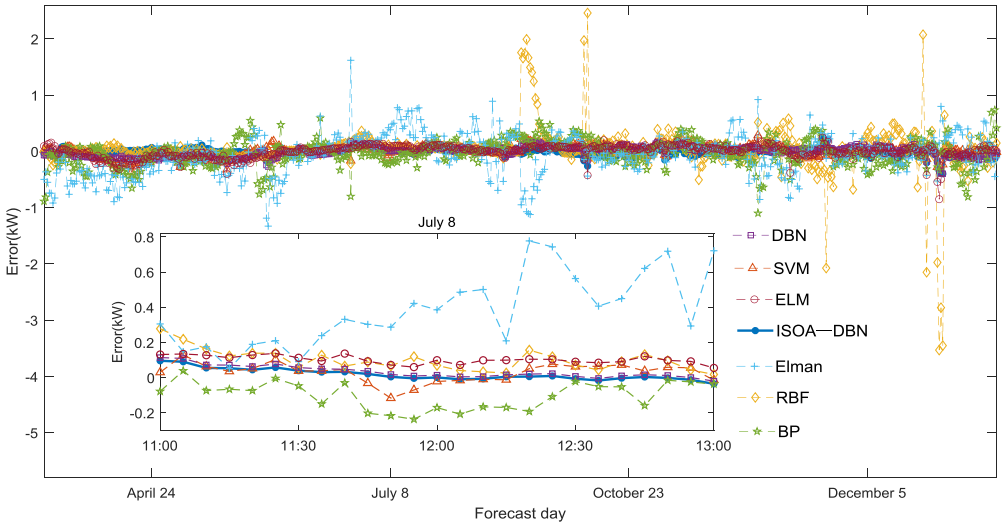

FIGURE 15. Prediction error of different seasons.

TABLE 7. Prediction error index in different seasons.

Season	Error	ISOA-DBN	DBN	SVM	ELM	RBF	Elman	BP
Autumn	RMSE(MW)	0.045	0.111	0.140	0.134	0.067	0.445	0.294
	MAPE(%)	0.751	3.028	3.728	3.334	1.164	8.627	5.693
Winter	RMSE(MW)	0.043	0.055	0.059	0.073	0.102	0.359	0.161
	MAPE(%)	0.985	1.390	1.690	2.336	2.839	9.018	3.343
Spring	RMSE(MW)	0.06	0.088	0.115	0.093	0.756	0.322	0.274
	MAPE(%)	1.51	2.184	2.729	2.372	6.977	4.862	4.687
Summer	RMSE(MW)	0.081	0.094	0.108	0.13	0.74	0.295	0.328
	MAPE(%)	1.573	2.083	1.621	2.168	11.286	6.073	6.028

proposed model are closer to the actual values in different seasons, showing better prediction performance. Compared with the six methods of DBN, SVM, ELM, RBF, Elman, and BP, the RMSE indicators of the proposed prediction method

(considering autumn an example) decrease by 0.066, 0.095, 0.089, 0.022, 0.4, and 0.249 KW, respectively. The MAPE indicators decrease by 2.277%, 2.977%, 2.583%, 0.413%, 7.876%, and 4.942%. Therefore, the proposed method has better adaptability to different seasons.

VI. CONCLUSION

In connection with the current research hotspot of deep learning algorithm, the ISOA-DBN prediction model is proposed. By analyzing the experimental results of the model under different weather types and seasons, the following conclusions were drawn:

1) A scheme of using FCBF algorithm to screen forecast model input meteorological feature set is proposed. This approach not only effectively determines the most relevant meteorological features corresponding to PV power generation power, but also avoids the redundancy problem among selected meteorological features.

2) The similarity in the distance and shape of the predicted day and its corresponding similar day is considered comprehensively, and the weight of meteorological parameters is determined by the standard deviation method. The optimum similar day selection method for the comprehensive similarity index is proposed by combining Euclidean distance with the gray correlation analysis method, which accurately realizes the selection of similar day.

3) The proposed ISOA algorithm optimizes DBN model parameters,, thereby improving the prediction performance of the model.

4) Finally, the actual PV power generation scenarios in different weather and seasons are considered. The proposed ISOA-DBN prediction model is compared with DBN, SVM, ELM, RBF, Elman, BP, and six other classical methods for analysis. The results show that the proposed method has good adaptability in both experimental scenarios and shows better prediction performance.

REFERENCES

[1] F. Wang, Z. Xuan, Z. Zhen, K. Li, T. Wang, and M. Shi, "A day-ahead PV power forecasting method based on LSTM-RNN model and time correlation modification under partial daily pattern prediction framework," *Energy Convers. Manage.*, vol. 212, May 2020, Art. no. 112766.

[2] P. Lin, Z. Peng, Y. Lai, S. Cheng, Z. Chen, and L. Wu, "Short-term power prediction for photovoltaic power plants using a hybrid improved Kmeans-GRA-Elman model based on multivariate meteorological factors and historical power datasets," *Energy Convers. Manage.*, vol. 177, pp. 704–717, Dec. 2018.

[3] J. Liu, W. Fang, X. Zhang, and C. Yang, "An improved photovoltaic power forecasting model with the assistance of aerosol index data," *IEEE Trans. Sustain. Energy*, vol. 6, no. 2, pp. 434–442, Apr. 2015.

[4] J. C. Richstein and S. S. Hosseinioun, "Industrial demand response: How network tariffs and regulation (do not) impact flexibility provision in electricity markets and reserves," *Appl. Energy*, vol. 278, Nov. 2020, Art. no. 115431.

[5] M. McPherson and B. Stoll, "Demand response for variable renewable energy integration: A proposed approach and its impacts," *Energy*, vol. 197, Apr. 2020, Art. no. 117205.

[6] A. Vinayagam, A. A. Alqumsan, K. S. V. Swarna, S. Y. Khoo, and A. Stojcevski, "Intelligent control strategy in the islanded network of a solar PV microgrid," *Electr. Power Syst. Res.*, vol. 155, pp. 93–103, Feb. 2018.

[7] K. Roy, K. K. Mandal, and A. C. Mandal, "Ant-lion optimizer algorithm and recurrent neural network for energy management of micro grid connected system," *Energy*, vol. 167, pp. 402–416, Jan. 2019.

[8] M. S. Nazir, A. N. Abdalla, Y. Wang, Z. Chu, J. Jie, P. Tian, M. Jiang, I. Khan, P. Sanjeevikumar, and Y. Tang, "Optimization configuration of energy storage capacity based on the microgrid reliable output power," *J. Energy Storage*, vol. 32, Dec. 2020, Art. no. 101866.

[9] A. Ketabi, A. Karimizadeh, and M. Shahidehpour, "Optimal generation units start-up sequence during restoration of power system considering network reliability using bi-level optimization," *Int. J. Electr. Power Energy Syst.*, vol. 104, pp. 772–783, Jan. 2019.

[10] C. L. T. Borges, "An overview of reliability models and methods for distribution systems with renewable energy distributed generation," *Renew. Sustain. Energy Rev.*, vol. 16, no. 6, pp. 4008–4015, Aug. 2012.

[11] A. Maleki, M. A. Nazari, and F. Pourfayaz, "Harmony search optimization for optimum sizing of hybrid solar schemes based on battery storage unit," *Energy Rep.*, vol. 6, pp. 102–111, Dec. 2020.

[12] N. Pearre and L. Swan, "Combining wind, solar, and in-stream tidal electricity generation with energy storage using a load-perturbation control strategy," *Energy*, vol. 203, Jul. 2020, Art. no. 117898.

[13] C. Byers and A. Botterud, "Additional capacity value from synergy of variable renewable energy and energy storage," *IEEE Trans. Sustain. Energy*, vol. 11, no. 2, pp. 1106–1109, Apr. 2020.

[14] A. Azizivahed, A. Arefi, S. Ghavidel, M. Shafie-Khah, L. Li, J. Zhang, and J. P. S. Catalao, "Energy management strategy in dynamic distribution network reconfiguration considering renewable energy resources and storage," *IEEE Trans. Sustain. Energy*, vol. 11, no. 2, pp. 662–673, Apr. 2020.

[15] F. Barbieri, S. Rajakaruna, and A. Ghosh, "Very short-term photovoltaic power forecasting with cloud modeling: A review," *Renew. Sustain. Energy Rev.*, vol. 75, pp. 242–263, Aug. 2017.

[16] A. Dubey and S. Santoso, "On estimation and sensitivity analysis of distribution circuit's photovoltaic hosting capacity," *IEEE Trans. Power Syst.*, vol. 32, no. 4, pp. 2779–2789, Jul. 2017.

[17] T. Ma, H. Yang, and L. Lu, "Solar photovoltaic system modeling and performance prediction," *Renew. Sustain. Energy Rev.*, vol. 36, pp. 304–315, Aug. 2014.

[18] C. Monteiro, L. A. Fernandez-Jimenez, I. J. Ramirez-Rosado, A. Muñoz-Jimenez, and P. M. Lara-Santillan, "Short-term forecasting models for photovoltaic plants: Analytical versus soft-computing techniques," *Math. Problems Eng.*, vol. 2013, pp. 1–9, Oct. 2013.

[19] F. Almonacid, P. J. Pérez-Higueras, E. F. Fernández, and L. Hontoria, "A methodology based on dynamic artificial neural network for short-term forecasting of the power output of a PV generator," *Energy Convers. Manage.*, vol. 85, pp. 389–398, Sep. 2014.

[20] U. K. Das, K. S. Tey, M. Seyedmahmoudian, S. Mekhilef, M. Y. I. Idris, W. Van Deventer, B. Horan, and A. Stojcevski, "Forecasting of photovoltaic power generation and model optimization: A review," *Renew. Sustain. Energy Rev.*, vol. 81, pp. 912–928, Jan. 2018.

[21] R. Huang, T. Huang, R. Gadh, and N. Li, "Solar generation prediction using the ARMA model in a laboratory-level micro-grid," in *Proc. IEEE 3rd Int. Conf. Smart Grid Commun. (SmartGridComm)*, Nov. 2012, pp. 528–533.

[22] Y. Li, J. Zhang, J. Xiao, and Y. Tan, "Short-term prediction of the output power of PV system based on improved grey prediction model," in *Proc. Int. Conf. Adv. Mech. Syst.*, Aug. 2014, pp. 547–551.

[23] S. T. Sarena, K.-L. Lian, T.-H. Chen, T.-D. Huang, K.-S. Tung, Y.-R. Chang, Y. D. Lee, and Y.-H. Ho, "Very short term solar irradiance prediction for a microgrid system in taiwan based on hybrid of support vector regression and grey theory," in *Proc. 3rd Int. Conf. Electric Power Energy Convers. Syst.*, Oct. 2013, pp. 1–6.

[24] H. T. C. Pedro and C. F. M. Coimbra, "Assessment of forecasting techniques for solar power production with no exogenous inputs," *Sol. Energy*, vol. 86, no. 7, pp. 2017–2028, Jul. 2012.

[25] S. Wang, Y. Wang, Y. Cheng, S. Sun, N. Wang, P. Yu, and S. Wang, "An improved model for power prediction of PV system based on elman neural networks," in *Proc. Asia Energy Electr. Eng. Symp. (AEEES)*, May 2020, pp. 902–907.

[26] G.-Q. Lin, L.-L. Li, M.-L. Tseng, H.-M. Liu, D.-D. Yuan, and R. R. Tan, "An improved moth-flame optimization algorithm for support vector machine prediction of photovoltaic power generation," *J. Cleaner Prod.*, vol. 253, Apr. 2020, Art. no. 119966.

[27] Y. Zhou, N. Zhou, L. Gong, and M. Jiang, "Prediction of photovoltaic power output based on similar day analysis, genetic algorithm and extreme learning machine," *Energy*, vol. 204, Aug. 2020, Art. no. 117894.

[28] Y. Jiang, Y. Yang, Q. Wu, X. Chi, and J. Miao, "Research on predicting the short-term output of photovoltaic (PV) based on extreme learning machine model and improved similar day," in *Proc. IEEE Innov. Smart Grid Technol. Asia (ISGT Asia)*, May 2019, pp. 3691–3695.
[29] J. Alsarraf, H. Moayedi, A. S. A. Rashid, M. A. Muazu, and A. Shahsavar, "Application of PSO-ANN modelling for predicting the exergetic performance of a building integrated photovoltaic/thermal system," *Eng. Comput.-Germany*, vol. 36, no. 2, pp. 633–646, 2020.
[30] Z.-F. Liu, L.-L. Li, M.-L. Tseng, and M. K. Lim, "Prediction short-term photovoltaic power using improved chicken swarm optimizer–Extreme learning machine model," *J. Cleaner Prod.*, vol. 248, Mar. 2020, Art. no. 119272.
[31] D. Niu, K. Wang, L. Sun, J. Wu, and X. Xu, "Short-term photovoltaic power generation forecasting based on random forest feature selection and CEEMD: A case study," *Appl. Soft Comput.*, vol. 93, Aug. 2020, Art. no. 106389.
[32] Z. Yang, M. Mourshed, K. Liu, X. Xu, and S. Feng, "A novel competitive swarm optimized RBF neural network model for short-term solar power generation forecasting," *Neurocomputing*, vol. 397, pp. 415–421, Jul. 2020.
[33] Y. Wang, W. Fu, and H. Xue, "DMCS-WNN prediction method of photovoltaic power generation by considering solar radiation and chaotic feature extraction," *Proc. CSEE*, vol. 39, pp. 63–71, Aug. 2019.
[34] M. Pan, C. Li, R. Gao, Y. Huang, H. You, T. Gu, and F. Qin, "Photovoltaic power forecasting based on a support vector machine with improved ant colony optimization," *J. Cleaner Prod.*, vol. 277, Dec. 2020, Art. no. 123948.
[35] G. Chitalia, M. Pipattanasomporn, V. Garg, and S. Rahman, "Robust short-term electrical load forecasting framework for commercial buildings using deep recurrent neural networks," *Appl. Energy*, vol. 278, Nov. 2020, Art. no. 115410.
[36] C. Fan, C. Ding, J. Zheng, L. Xiao, and Z. Ai, "Empirical mode decomposition based multi-objective deep belief network for short-term power load forecasting," *Neurocomputing*, vol. 388, pp. 110–123, May 2020.
[37] M. Alipour, J. Aghaei, M. Norouzi, T. Niknam, S. Hashemi, and M. Lehtonen, "A novel electrical net-load forecasting model based on deep neural networks and wavelet transform integration," *Energy*, vol. 205, Aug. 2020, Art. no. 118106.
[38] B. Gu, T. Zhang, H. Meng, and J. Zhang, "Short-term forecasting and uncertainty analysis of wind power based on long short-term memory, cloud model and non-parametric kernel density estimation," *Renew. Energy*, vol. 164, pp. 687–708, Feb. 2021.
[39] R. Yu, J. Gao, M. Yu, W. Lu, T. Xu, M. Zhao, J. Zhang, R. Zhang, and Z. Zhang, "LSTM-EFG for wind power forecasting based on sequential correlation features," *Future Gener. Comput. Syst.*, vol. 93, pp. 33–42, Apr. 2019.
[40] K. Wang, X. Qi, H. Liu, and J. Song, "Deep belief network based k-means cluster approach for short-term wind power forecasting," *Energy*, vol. 165, pp. 840–852, Dec. 2018.
[41] C. Zhang, Y. He, L. Yuan, and S. Xiang, "Analog circuit incipient fault diagnosis method using DBN based features extraction," *IEEE Access*, vol. 6, pp. 23053–23064, May 2018.
[42] Y. Zhang, G. Pan, Y. Zhao, Q. Li, and F. Wang, "Short-term wind speed interval prediction based on artificial intelligence methods and error probability distribution," *Energy Convers. Manage.*, vol. 224, Nov. 2020, Art. no. 113346.
[43] E. Wang, N. Alp, J. Shi, C. Wang, X. Zhang, and H. Chen, "Multi-criteria building energy performance benchmarking through variable clustering based compromise TOPSIS with objective entropy weighting," *Energy*, vol. 125, pp. 197–210, Apr. 2017.
[44] G. E. Hinton, "Reducing the dimensionality of data with neural networks," *Science*, vol. 313, no. 5786, pp. 504–507, Jul. 2006.
[45] G. E. Hinton, S. Osindero, and Y.-W. Teh, "A fast learning algorithm for deep belief nets," *Neural Comput.*, vol. 18, no. 7, pp. 1527–1554, Jul. 2006.
[46] Y. Li, L. Wang, and L. Jiang, "Rolling bearing fault diagnosis based on DBN algorithm improved with PSO," *J. Vib. Shock*, vol. 39, pp. 89–96, May 2020.
[47] G. Dhiman and V. Kumar, "Seagull optimization algorithm: Theory and its applications for large-scale industrial engineering problems," *Knowl.-Based Syst.*, vol. 165, pp. 169–196, Feb. 2019.
[48] H. Wang, Z. Wu, S. Rahnamayan, Y. Liu, and M. Ventresca, "Enhancing particle swarm optimization using generalized opposition-based learning," *Inf. Sci.*, vol. 181, no. 20, pp. 4699–4714, Oct. 2011.

WEI HU received the M.Sc. degree from the Kunming University of Science and Technology, in 2016. He is currently pursuing the Ph.D. degree with Xinjiang University. His current research interests include renewable energy forecasting and capacity configuration of the energy storage system.

XINYAN ZHANG received the Ph.D. degree from Xi'an Jiaotong University, in 2010. She is currently a Professor and a Doctoral Supervisor with the School of Electrical Engineering, Xinjiang University. Her research interests are new energy grid connection analysis and fault diagnosis of power electronic systems.

LIJUAN ZHU received the M.Sc. degree from the Kunming University of Science and Technology, in 2016. She is currently a Lecturer with the Xinjiang Institute of Technology. Her research interests are artificial intelligence and image processing.

ZHENEN LI received the M.Sc. degree from the Lanzhou University of Science and Technology. He is currently pursuing the Ph.D. degree with Xinjiang University. His research interests are applications, as well as testing and fault diagnosis of power equipment.